Int J Adv Manuf Technol (2016) 87:2951–2965
DOI 10.1007/s00170-016-8656-7

ORIGINAL ARTICLE

Non-isothermal deformation behavior and FE simulation of ultrahigh strength BR1500HS steel in hot stamping process

Wurong Wang[1] · **Lei Zhang**[1] · **Mengxuan Guo**[1] · **Lei Huang**[1] · **Xicheng Wei**[1]

Received: 14 September 2015 / Accepted: 20 March 2016 / Published online: 8 April 2016

Abstract In the current work, the effects of initial deformation temperature and strain rate on flow behavior and microstructure of boron-alloyed steel after non-isothermal deformation were investigated. Based on the stress-strain curve obtained in the non-isothermal tensile experiment with a Gleeble 3500 system, finite element software was used to carry out the thermal mechanical coupled simulation of hot stamping process, which was further validated by hot stamping experiment of a V-channel part. The results indicate that the forming force was higher than that of the isothermal deformation. It was also observed that the initial stamping temperature should be above 750 °C, and the holding and quenching time should be up to 15 s in hot stamping process according to finite element (FE) simulation. Finally, the results obtained from hot stamping experiments are in good consistency with the simulation; thus, it reveals that the FE modeling of non-isothermal hot stamping process is reliable.

Keywords Hot stamping · Non-isothermal deformation · Boron-alloyed steel · Numerical simulation

1 Introduction

In order to increase the crashworthiness of cars and save weight in the automotive industry, more and more body parts are manufactured out of high-strength steels. According to the research of Karbasian et al. [1], hot stamping of high-strength steels such as manganese boron steel (22MnB5) is more and more widely applied to bumper beams, A-pillars, B-pillars, etc., due to its excellent formability [2], low springback, and ultrahigh strength of hot-stamped components. In hot stamping, the steel passes a two-step microstructural transformation from ferrite-pearlite into austenite by means of a specific heat treatment followed by a martensitic phase transformation during quenching in the stamping press, thus it is possible to produce parts with tensile strength of up to 1500 MPa [3].

Naderi et al. [4] found that hot stamping was a non-isothermal high-temperature forming process, in which the sheet temperature was constantly changing, and both forming and phase transformations were almost simultaneously performed in a single step. Therefore, studying the non-isothermal deformation behavior at high temperature has an important guiding significance on the determination of hot stamping process as well as the improvement of simulation accuracy of hot stamping process both in theory and practice.

Finite element (FE) simulation is becoming an increasingly important tool in the process design for structural automotive components which are manufactured using hot stamping. And, the use of the finite element method has received much attention over the past years. Using the finite element analysis, which takes the deformation and strengthening induced by the cooling and phase transformation into account, Kim et al. [5] studied the deformation behavior during the proposed hot stamping process. Li et al. [6] designed the hot stamping processes and Won et al. [7] manufactured car body parts with tailored properties by using finite element technology. It was proposed by Tekkaya et al. [8] that the phenomena during hot stamping can be divided into heat transfer between hot sheet,

✉ Wurong Wang
wrwang@shu.edu.cn

[1] School of Materials Science and Engineering, Shanghai University, Shanghai, China

Table 1 Chemical compositions of the investigated BR1500HS steel

Element	C	Si	Mn	Cr	Mo	B	S	P	Fe
wt. %	0.23	0.254	1.35	0.19	0.04	0.003	0.006	0.015	Balanced

cold die and environment, plastic deformation of the sheet, and phase transformation of sheet due to cooling in the die. Thus, a thermal mechanical coupled simulation is suggested to consider these phenomena adequately for obtaining the accurate results.

The isothermal hot deformation has been the focus of many researchers. Abbasi et al. [9] has studied the effect of strain rate and deformation temperature on the characteristics of isothermally hot-compressed boron-alloyed steel and reported that at a constant strain rate, the hardness and martensite start temperature (M_s) normally increase as the deformation temperature increases and it is also observed that higher strain rates increase the hardness and flow stress, although a clear effect of strain rate on M_s is not observed. Min et al. [10] has investigated the effect of thermo-mechanical process on the microstructure and secondary deformation behavior in isothermally deformed 22MnB5 steels. They concluded that as the steel was deformed at 923 K, deformation-induced ferrite transformation (DIFT) occurred even when a small strain of 0.044 was applied, and the volume fraction of deformation-induced ferrite (DIF) increases with increasing strain level applied. Moreover, when deformed at 693 K, deformation-induced bainite transformation (DIBT) was observed when the applied strain was larger than 0.109. The incubation period for DIFT is shorter than that for DIBT, but the DIBT proceeds much faster than DIFT. Naderi et al. analyzed the effects of non-isothermal deformation on martensitic transformation in 22MnB5 steel and reported that a higher initial deformation temperature resulted in a higher martensite fraction of the microstructure. Furthermore, they concluded that by applying larger amounts of strain as well as higher force levels, not only the martensite start temperature but also the amount of martensite was reduced. Further analyses to isothermal versus non-isothermal hot compression process has shown that higher forming loads as well as M_s and M_f temperatures are the characteristics of the non-isothermal process of 22MnB5 steel [11]. Additionally, following the isothermal compression process by quenching resulted in a fully martensitic microstructure.

However, as an important input for improving the simulation accuracy of hot stamping process, the stress-strain behavior under non-isothermal deformation of manganese boron steel has not been thoroughly investigated. Therefore, the effects of strain rate and initial deformation temperature on the non-isothermal deformation behavior of a boron-alloyed steel (BR1500HS) were conducted in this study. Moreover, finite element simulation was used for simulating the actual hot stamping process. At the same time, the influences of process parameters such as the initial deformation temperature and the holding time on the mechanical properties and final microstructure of the hot-stamped parts were investigated. Finally, hot stamping experiments were carried out to validate the correctness of the FE modeling.

2 Material and experiment

2.1 Material

The investigated material is BR1500HS steel with a thickness of 1.8 mm. The chemical compositions are listed in Table 1 and the microstructure of plates consisting of 75 vol.% (±5 %) ferrite and 25 vol.% (±5 %) pearlite in as-received condition is shown in Fig. 1. It can be seen that BR1500HS steel is a 22MnB5 type manganese boron steel specifically designed for hot stamping.

2.2 Non-isothermal tensile test

The non-isothermal tensile tests of the BR1500HS steel at elevated temperatures were conducted on a Gleeble 3500 thermo-mechanical simulation system. According to the

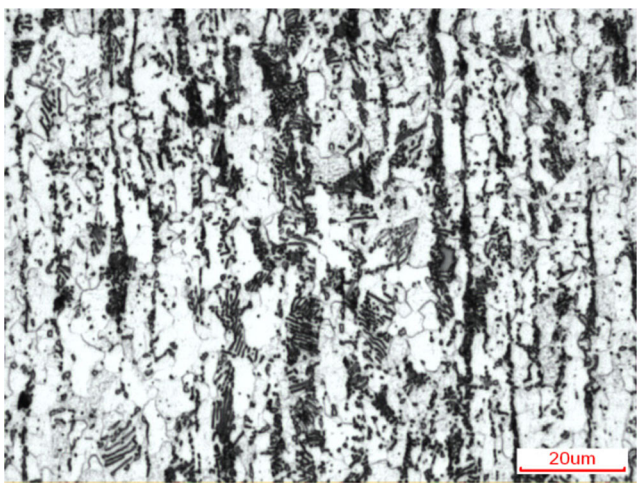

Fig. 1 Microscopic morphology of as-received BR1500HS steel

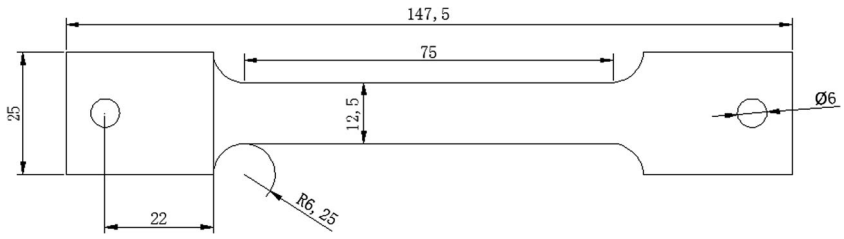

Fig. 2 Illustration for dimensions of the tensile specimens (unit in mm)

standard GB/T4338-2006, the dimensions of the tensile specimens are illustrated in Fig. 2.

In all of the tensile tests, the samples were first austenitized at 920 °C for 5 min and then quenched to the various initial deformation temperatures of 900, 850, 800, 750 °C, respectively. And then, the samples were simultaneously deformed and cooled from the initial deformation temperatures to 700 °C, in which the strain rates were 0.15, 1.5, and 15 s^{-1} and the cooling rate was 50 °C/s approximately. In Fig. 3, the detailed procedures for the tests are illustrated schematically.

2.3 FE modeling of non-isothermal hot stamping process for V-channel part

The numerical simulations for the V-channel part were carried out to investigate the hot stamping process and the FE model was illustrated in Fig. 4. The simulation of a hot stamping process could be divided into four stages, as shown in Fig. 5. The gravity stage was modeled as implicit and used a mechanical field only. Holding and stamping stages used both mechanical and thermal fields. Stamping should be completed while the blank was still in the austenite phase, and no phase transformation was desired in this stage. And, the quenching stage used thermal and microstructure evolution fields. The detailed material properties and simulation conditions were shown in Table 2.

2.4 Hot stamping experiment of the V-channel part

The part illustrated in Fig. 6 was based on a typical V-channel section from a B-pillar part. The hot stamping process of the V-channel part was completed in the experimental setup of hot forming, which was presented in Fig. 7. In hot stamping experiments, the blank was austenitized at 920 °C for 5 min in a furnace to guarantee a complete, homogenous austenitization, and then transferred to the experimental setup within 10 s. Additionally, in the hot stamping process, the stamping speed was 100 mm/s, the holding force was 500 kN, the quenching time was set to be 15 s, and the flow rate of the cooling

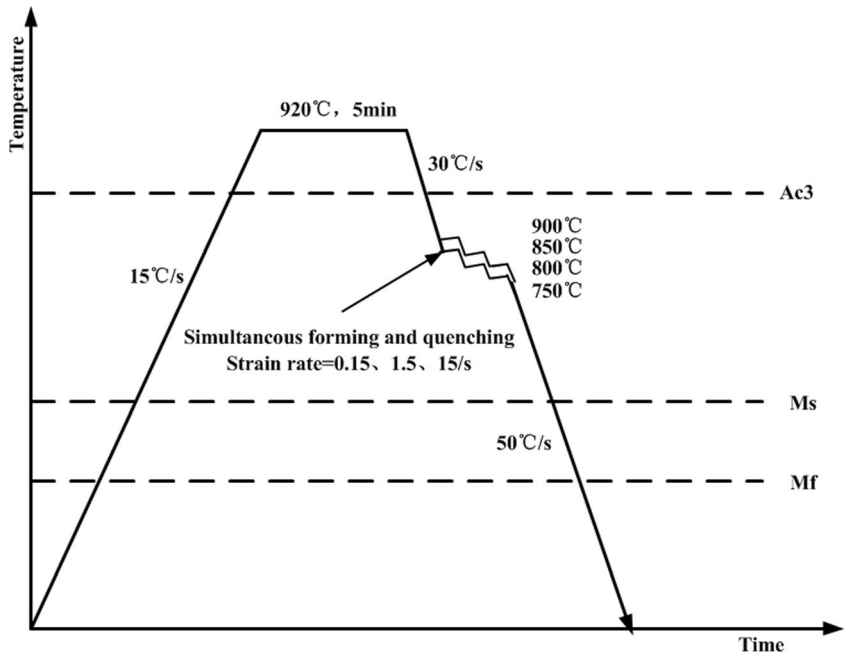

Fig. 3 Schematic of the procedure for non-isothermal deformation process

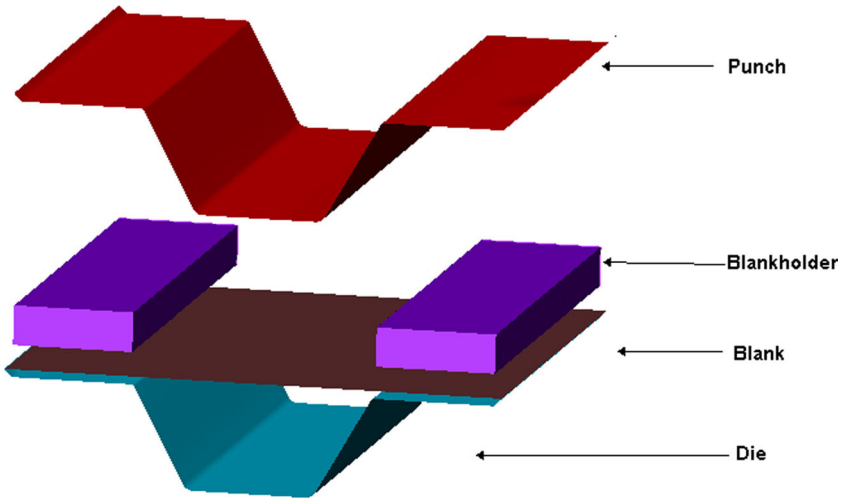

Fig. 4 FE models of hot stamping process

water was 5 mm/s. Finally, the microstructure, tensile strength and thinning of formed parts were measured, and the measuring specimens were taken from the bottom, the flange, and the sidewall of the stamping parts (Fig. 8), which were used to validate the accuracy of the FE simulation.

3 Non-isothermal deformation behavior of BR1500HS steels

3.1 The effect of initial deformation temperatures

One of the key factors during hot stamping process is the initial deformation temperature. When the heated blanks are transferred from the furnace into the die, the temperature of the hot blank will drop in no time. Thus, the deformation is not performed at the austenitization temperature, but instead it is performed at lower temperature, so called the initial deformation temperature.

Therefore, the initial deformation temperatures in non-isothermal tensile test were selected from 750 to 900 °C in 50 °C intervals, which were lower than the austenitization temperature. The influence of the initial deformation temperature on the flow properties of BR1500HS steel was investigated under different temperatures from 750 to 900 °C and different strain rates of 0.15, 1.5, and 15 s^{-1}, respectively. Figure 9 shows the true stress-strain curves at different initial deformation temperatures, with the strain rate of 15 s^{-1}. It can be seen that initial deformation temperature has a significant influence on the flow stress of BR1500HS steel. Increasing initial deformation temperature leads to a decrease in peak stress and work hardening, resulting in a noticeable decrease of slope of the true stress-strain curves. Fan et al. [12] suggested that this may be related to the effect of dynamic recovery caused by the annihilation of dislocations when temperature is increased, and correspondingly, the matrix is softened, which was also mentioned in the work of Nes et al. [13]. When the temperature dropped to 750 °C, the effect of work hardening was extremely obvious and the resistance strength to deformation was very high, up to 360 MPa. Therefore, the shorter the transfer time of blank sheet in hot stamping process is, the better the purpose of achieving a higher initial deformation temperature will be. Nevertheless, the results also show that the forming force of non-isothermal deformed sample was higher than that of the isothermally deformed BR1500HS

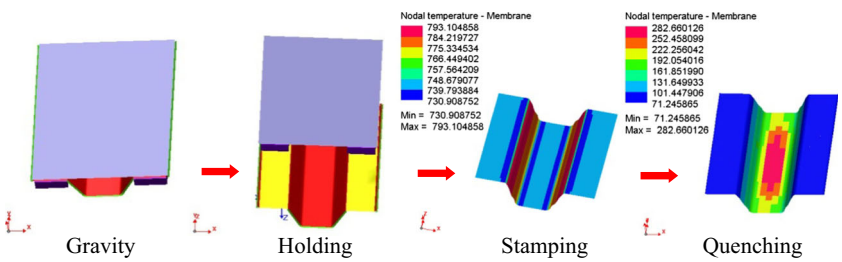

Fig. 5 Stages of a hot stamping simulation

Table 2 Material properties and simulation conditions

Material	BR1500HS
Thickness (mm)	1.8
Properties	
Density (kg/m^3)	7850
Young's modulus (GPa)	210
Poisson's ratio	0.3
Linear expansion (°C)	2×10^{-5}
Simulation conditions	
Punch speed (mm/s)	100
Tool temperature (°C)	25
Initial stamping temperature	700, 750, 800 °C
Holding and quenching time (s)	10, 15 s
Blank-holder force (kN)	500
Friction coefficient	0.3
Radiation conductance (W/m^2 K)	100

steel [14]. These can be related to the larger number of point and line (dislocations) defects produced during non-isothermal deformation and cooling process than that in isothermal forming process [15].

Additionally, the optical microscopy was used to observe the effect of initial deformation temperature on microstructure of non-isothermal deformed BR1500HS steel. Representative micrographs of BR1500HS steel at a strain rate of 1.5 s^{-1} and various initial deformation temperatures are given in Fig. 10. Figure 11 plots the hardness of BR1500HS steel at different temperatures. As shown in Fig. 10, the BR1500HS steel samples which were deformed at 900 °C show almost full martensite with hardness over 480 $HV_{0.3}$. However, when deformed at 800 °C, the ferrite appears and the hardness drops to 402 $HV_{0.3}$.

Thus, in non-isothermal deformation process, there appeared the deformation-induced ferrite transformation (DIFT). It is known that when deformation is applied to the austenite phase, its free energy will be increased, which en-

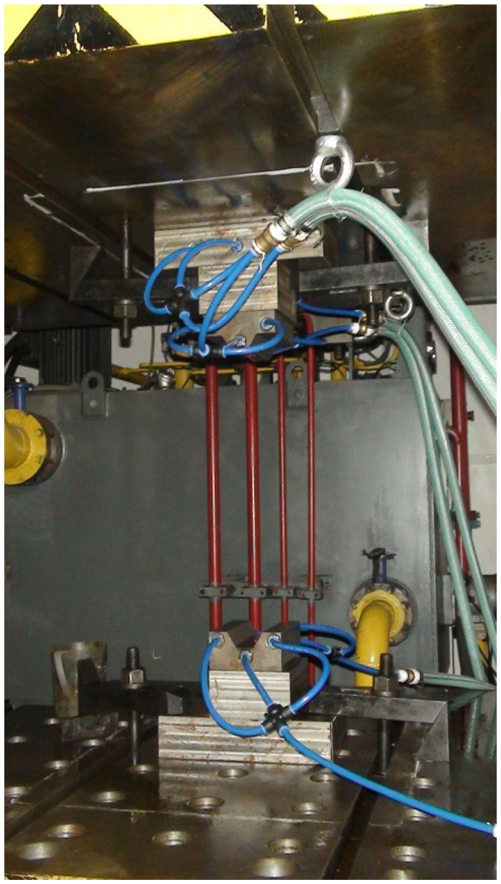

Fig. 7 The experimental setup of the V-channel stamping

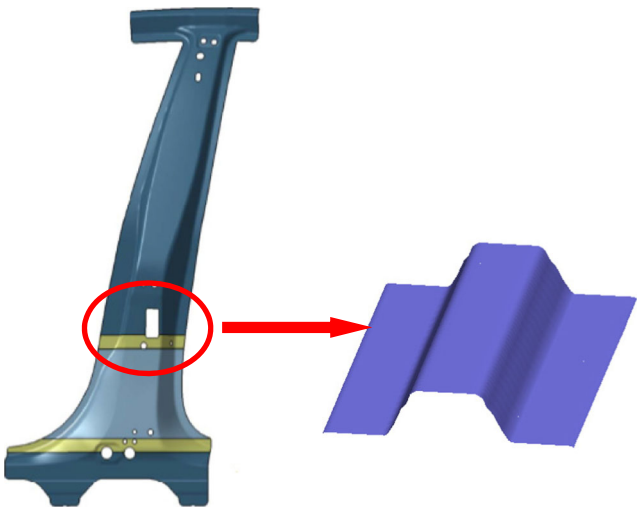

Fig. 6 Schematic of the V-channel part

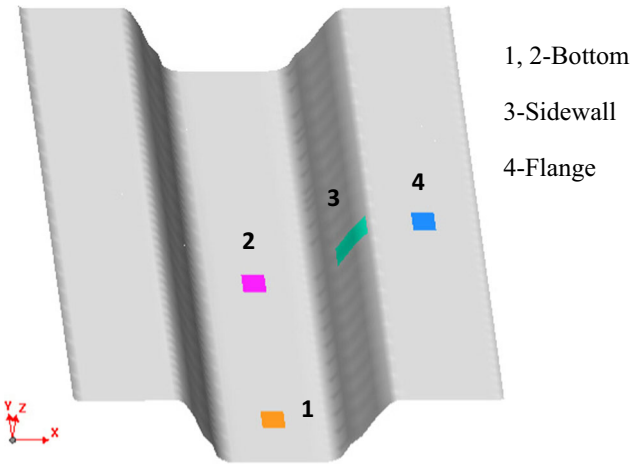

Fig. 8 Measuring sections of the V-channel part

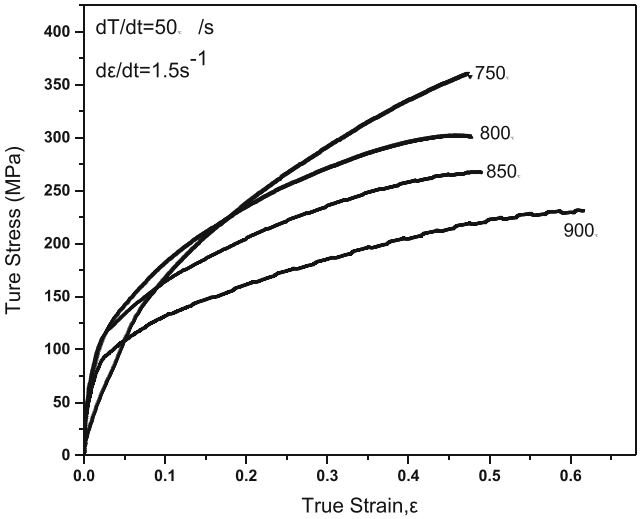

Fig. 9 Influence of initial deformation temperature on the flow property of BR1500HS

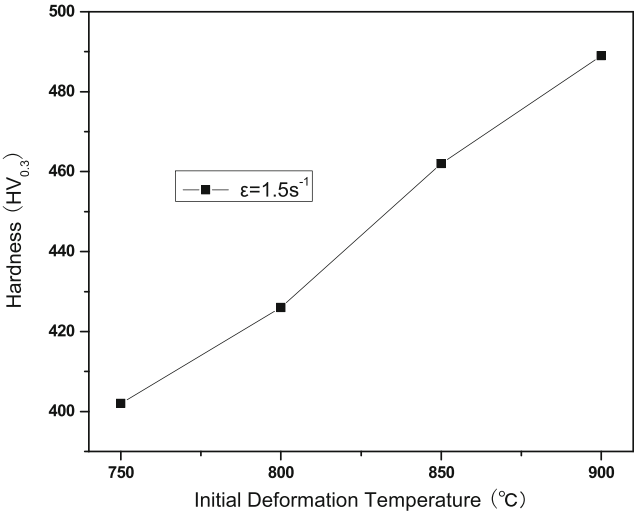

Fig. 11 Vickers hardness of BR1500HS steel specimens at different initial deformation temperatures with a strain rate of 1.5 s^{-1}

hances the driving force of ferrite transformation from the deformed austenite. Then, the deformation of austenite promotes its ferrite transformation. As seen from Fig. 10, the DIFT is enhanced when the initial deformation temperature decreased, which can be explained by the following aspects. First, decreasing temperature leads to an increasing driving force for ferrite transformation. Second, in the case of the same strain rate, the flow stress increases with decreasing deformation temperature. Therefore, more energy is introduced in the austenite and the effect of the DIFT is enhanced. Moreover, the deformed austenite is very unstable and will transform to ferrite in the following cooling process.

3.2 The effect of strain rate

The effect of strain rate on the flow properties of BR1500HS steel was investigated under different temperatures from 750 to 900 °C and different strain rates of 0.15, 1.5, and 15 s^{-1}, respectively. The flow curves are given in Fig. 12. It is observed that the increase of strain rate results in an enhancement of strength as well as the slope of the flow curves, as a consequence of an enforced work hardening of the material. Such effect can be related to the addition of dislocation density when the strain rate increases, as analyzed by Nagumo and Matsuda [16]. At the same time, the diffusional dependent

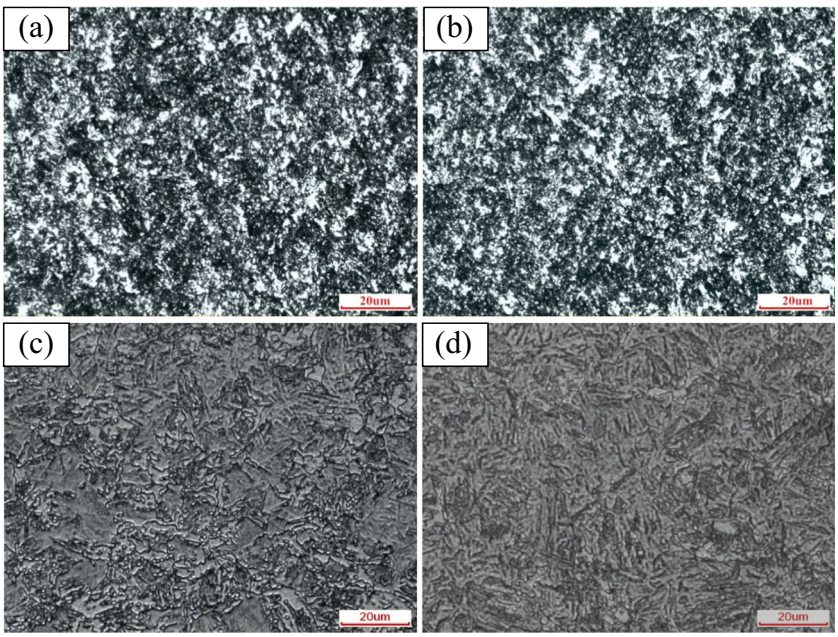

Fig. 10 Microscopic morphology of the BR1500HS steel specimens at different initial deformation temperatures with a strain rate of 1.5 s^{-1}. **a** 750 °C, **b** 800 °C, **c** 850 °C, **d** 900 °C

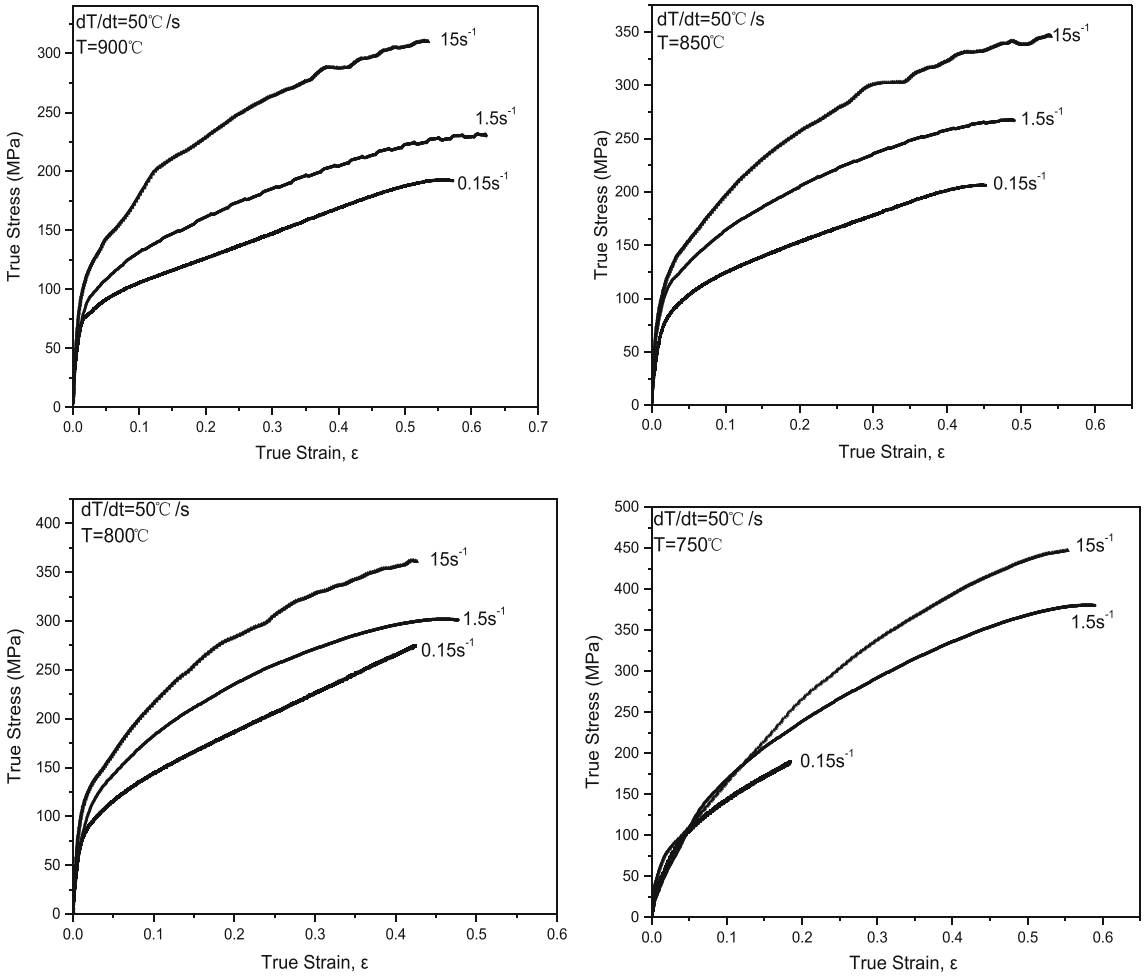

Fig. 12 Influence of strain rate on the flow properties of BR1500HS at different initial deformation temperatures

microstructural recovery processes takes place to balance the strain hardening [17].

As shown in the stress-strain curves, the increasing of strain rate leads to the increment of flow stress in the same strain level and the maximum of strain when necking tends to become bigger. According to Li et al. [6], the same tendency could appear in the isothermal deformation of BR1500HS steels. However, when the initial deformation temperature is 750 °C, the strain rate has a more significant impact on the formability of the material. It could be found that the test specimen is cracked even under a small amount of strain of 0.2 in a low strain rate (0.15 s^{-1}). When the strain rate increases, the maximum strain could be grown to about 0.5. What is more, the same phenome-

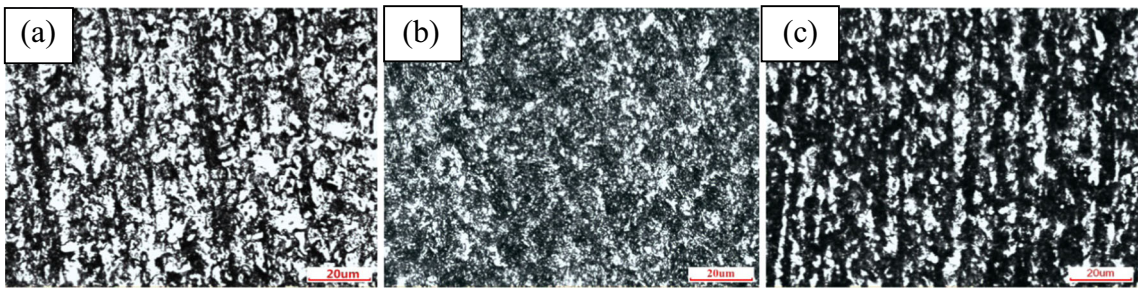

Fig. 13 Microscopic morphology of the BR1500HS steel specimens at different strain rates with an initial deformation temperature of 800 °C. **a** 0.15 s^{-1}, **b** 1.5 s^{-1}, **c** 15 s^{-1}

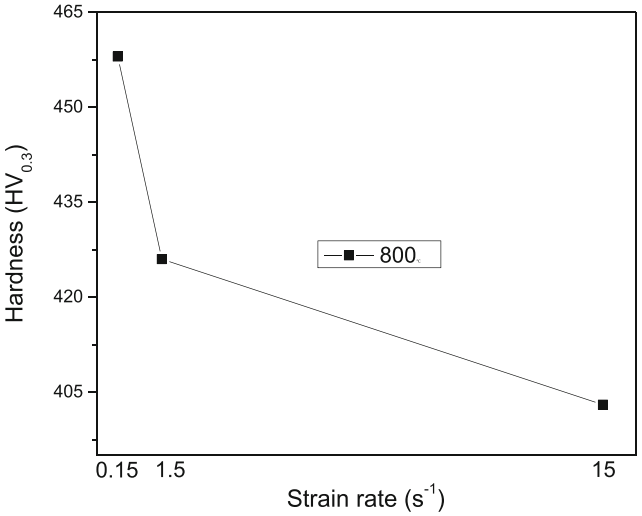

Fig. 14 Vickers hardness of BR1500HS steel specimens at different strain rate with an initial deformation temperatures of 800 °C

non is not obvious in isothermal deformation situation of BR1500HS steels at the temperature of 750 °C with a low strain rate. This may be because the effect of dynamic recovery is less obvious in non-isothermal deformation, leading to a relatively large forming force, and the heat generated by deformation within the unit time is very little, thus the test specimen was necked even at a small amount of strain. Therefore, when BR1500HS steel is formed at low initial deformation temperature (750 °C), it is suggested to increase the strain rate so as to avoid crack under small amount of strain.

The optical microscopy was used to investigate the influence of strain rate on microstructure of non-isothermal deformed BR1500HS steel. Representative micrographs of BR1500HS steel at an initial deformation temperature of 800 °C and various stain rates are given in Fig. 13. Figure 14 plots the microhardness of BR1500HS steel at different stain rates. As shown in Fig. 13, higher strain rates lead to less volume of martensite. When deformed at low strain rate of 0.15 s^{-1}, the sample shows almost full martensite with hardness over 450 $HV_{0.3}$. However, when deformed at higher strain rate of 15 s^{-1}, the hardness drops to 403 $HV_{0.3}$. This phenomenon could be related to more dislocations generated by higher strain rates. Because austenite becomes more mechanically stable at higher strain rates, the martensite start temperature (M_s) as well as martensitic transformation is reduced. Previous work by Naderi et al. [4] has shown that at temperature below 700 °C, higher strain rates resulted in more martensite in final microstructure. They concluded that the effect of mechanical stabilization is dominant at temperatures above 700 °C, while at lower temperatures, phase transformation is dominant.

4 Thermal-mechanical coupled simulation of V-channel hot stamping process

4.1 Thermal-mechanical-metallurgical coupled modeling

Based on the stress-stain curves obtained in the non-isothermal tensile experiment and some thermal parameters of BR1500HS steel, FE software PAMSTAMP 2G was used to carry out the thermal mechanical coupled simulation of hot stamping process. The thermal parameters of BR1500HS steel were partly referenced from the information about hot stamping steel 22MnB5 in material database of PAMSTAM 2G, and the detailed material properties and simulation conditions were listed in Table 2. The mechanical constitutive model used in this study was the stress-stain curves resulting from the non-isothermal tensile experiment in the Sect. 3. Figure 15 illustrates the imported flow curves using the "Points list" feature of the software.

As mentioned above in Sect. 2.3, the simulation of the V-channel hot stamping process in this study was divided into four stages: gravity, holding, forming, and quenching. In the process, thermal behavior is not considered during implicit simulation stages. The gravity stage was modeled as implicit and so only used a mechanical field. According to the actual hot stamping process, holding and forming stages used both mechanical and thermal fields. Forming has to be completed when the blank was still in the austenite phase; for this reason, no phase transformation was desired in forming, and the forming stage used no microstructure fields. While in the quenching stage, the austenite was transformed to martensite or maybe other phase, so thermal and microstructure evolution fields were used.

In the simulation process, to predict which phase transformation is occurred requires determination from a continuous cooling transformation (CCT) diagram. This study used JMatPro software to generate the CCT diagram for the BR1500HS material, which is shown in Fig. 16. The thick colored lines mark limits, where a certain phase transformations starts or ends (for color interpretation of the formability evaluation, the reader is suggested to refer to the electronic version of the article). For example, the martensite start temperature (M_s) is 389.1 °C, while the martensitic transformation finish temperature (M_f) is 277.3 °C. Those thin black solid lines in Fig. 16 are temperature histories starting from an austenitic state near 900 °C. From the CCT diagram, it is indicated that the cooling rate must be greater than 30 K/s, in order to avoid obtaining bainite and achieve more martensite.

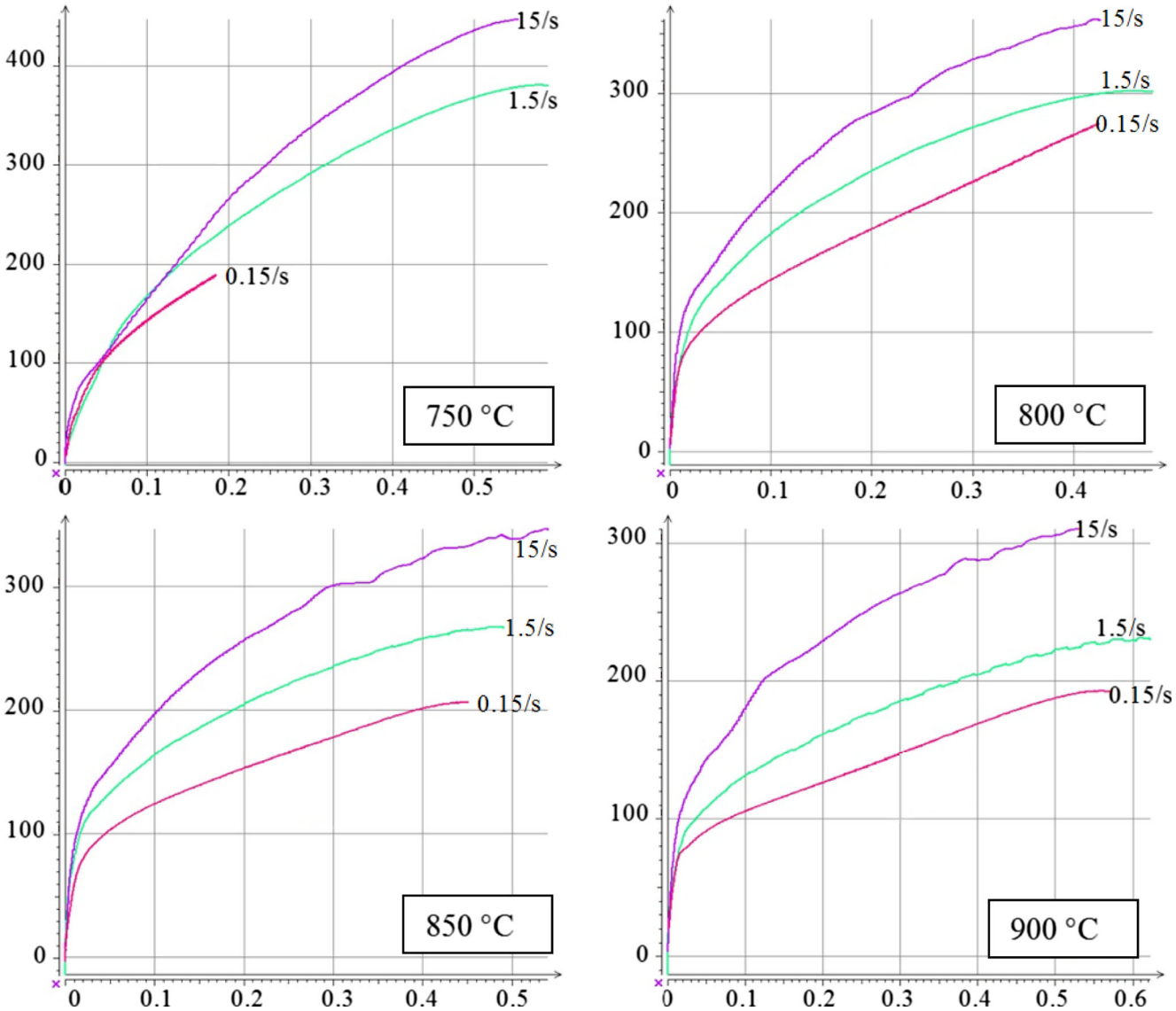

Fig. 15 The imported stain-stress curves of BR1500HS based on experiments

In metallurgical terms, a material is defined by proportions *Pi* of the various phases. In the simulation process, to predict the proportions *Pi* of the various phases, modes for describing metallurgical history, in other words to compute changes in the *Pi* proportions, is generalized to include Johnson-Mehl-Avrami type transformation kinetics and the Koistinen-Marburger law [18, 19]. A distinction is generally made between diffusion type phase and martensitic type transformation.

In terms of a diffusion type transformation (both the transformation of austenite to ferrite and transformation of austenite to bainite belong to this category), which occurs by nucleation and growth of a new phase inside the previous phase, the most frequently used model is that developed by Johnson, Mehl, and Avrami:

$$\frac{\mathrm{d}Pi}{dt} = n\left(\frac{\overline{P}-P}{TR}\right)\left(\ln\left(\frac{\overline{P}}{\overline{P}-Pi}\right)\right)^{\frac{n-1}{n}}$$

where P is proportion obtained after an infinite time, and $\overline{P}$ is interpreted as the equilibrium value. TR is delay time associated with the reaction, and n is an exponent illustrating the reaction rate. Detailed theory describing this model and obtaining the parameters from the CCT diagram can be referenced to the related publication [19].

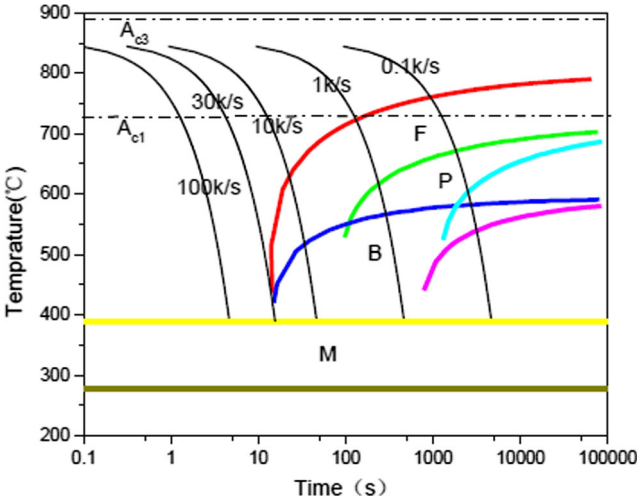

Fig. 16 CCT diagram of BR1500HS

In the case of a martensitic type transformation, formed phase proportion *Pi* depends only on current temperature θ in the form

$$Pi(\theta) = P\left(1-e^{b(\theta-\mathrm{Ms})}\right) \text{ for } \theta \leq \mathrm{Ms}$$

where P is the proportion obtained at an infinitely low temperature, frequently assimilated to 1. Parameters Ms and b characterize transformation start temperature and transformation rate, respectively.

With the abovementioned thermal-mechanical-metallurgical coupled modeling, effects of the initial stamping temperature and holding time were investigated to obtain main parameters in hot stamping process by analyzing the temperature distribution and microstructure transformation resulting from the simulation of the V-channel hot stamping process. Finally, hot stamping experiments were carried out to validate the correctness of the FE modeling.

4.2 Initial stamping temperature

The initial stamping temperature plays an important role in hot stamping process. On one hand, the cost of production will be high if the stamping temperature is too high. On the other hand, the resistance to deformation increases when the stamping temperature decreases, resulting in poor formability. Therefore, the initial stamping temperatures are selected from 700 to 800 °C in 50 °C intervals. Figure 17 shows the distributions of temperature of the part at different initial stamping temperatures with a holding and quenching time setting at 15 s. In Fig. 17, when the holding and quenching time is 0 s, the sidewall and bottom of the part exhibit a higher temperature than the flange area. This is mainly related to the well contact between the flange and the die, which improves the heat transfer from the flange to the die and the environment; on the contrary, the sidewall and bottom are cooled at lower cooling rate. Thus, the area of sidewall and bottom should be placed more cooling channels in die structure design in order to increase the cooling rate.

Figure 18 shows the microstructure distributions of the part at the end of quenching. It can be seen that when the initial stamping temperature was above 750 °C, the volume fractions of martensite reached 90 %. For the case of initial stamping temperature of 800 °C, the volume fractions of martensite reached 98 %. However, when the initial stamping temperature was 700 °C, the martensite volume fraction is lower than 90 % and a small quantity of bainite was detected.

Furthermore, the change of martensite volume fractions is plotted in Fig. 19 by selecting the typical elements of the part which are illustrated in Fig. 8 in hot stamping process with the initial stamping temperature of 800 °C. As shown in the curves, the flange (element 4) area of the part reaches the martensite start temperature (M_s) firstly, and it has full martensite in 5 s. However, the bottom (element 1, 2) area of the part reaches the M_s after 9 s and it still has not been fully transformed into martensite in 15 s. Thus, it is concluded

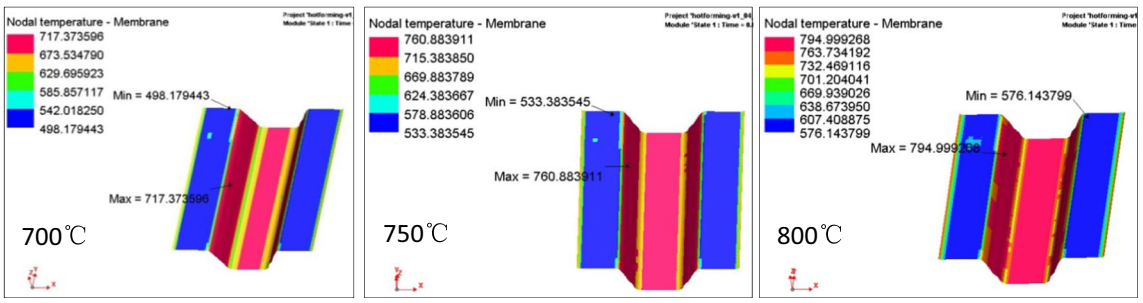

Fig. 17 Temperature distributions of the part before quenching

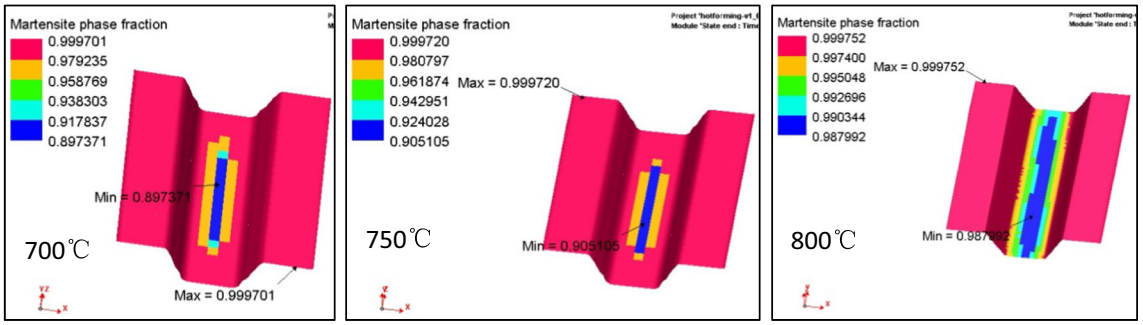

Fig. 18 Microstructure of the part at different initial stamping temperatures

that the holding and quenching time should be above 15 s in this working conditions.

4.3 Holding and quenching time

Another key factor of hot stamping process is the holding and quenching time with a fixed pressure. On one hand, the material can release its internal stress at this stage so as to reduce its springback. And on the other hand, enough time is required to let the microstructure of the steel transform from austenite to martensite. The influence of holding and quenching time on hot stamping process of BR1500HS steel was investigated under different times of 10 and 15 s with the initial stamping temperature of 800 °C.

Figures 20, 21, and 22 show the distributions of temperature, microstructure, and hardness of the part at the end of hot stamping under variable holding time. It is shown in Fig. 20 that the temperature of formed part was still very high in bottom and sidewall, up to 404 °C, with the holding and quenching time of 10 s. And, the volume fraction of martensite was only 1.3 % with a hardness of 321 HV in the bottom of the part, shown in Figs. 21 and 22. Due to the large die gap and poor heat dissipation conditions, the sidewall and bottom of the part cannot be cooled and quenched

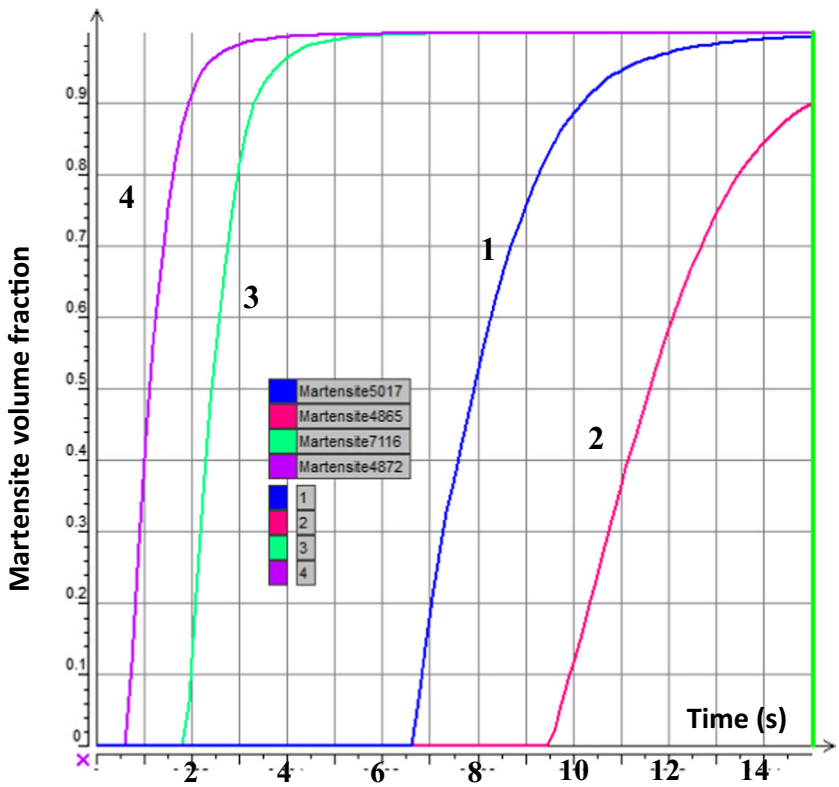

Fig. 19 Martensite volume fractions during forming of selected locations 1 to 4 (labeled in Fig. 8) with the initial stamping temperature of 800 °C

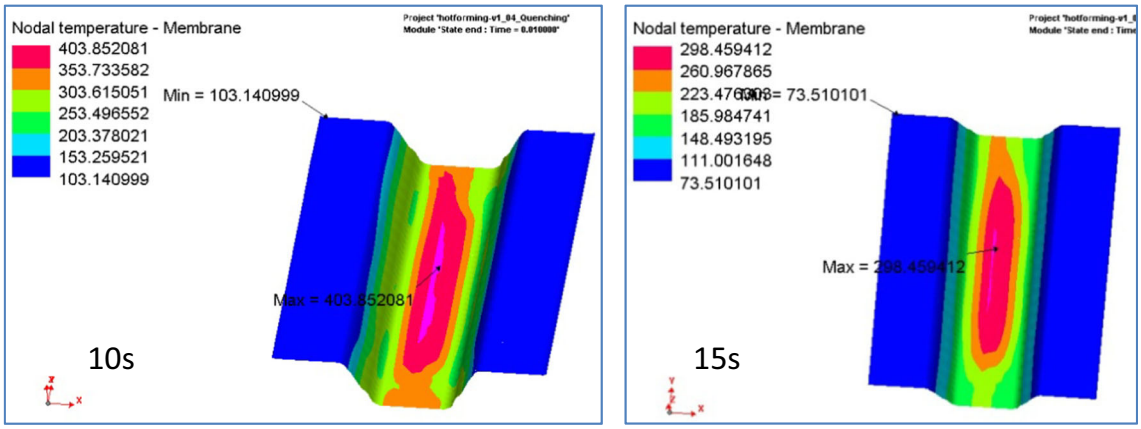

Fig. 20 Temperature distribution of the part at different holding and quenching time

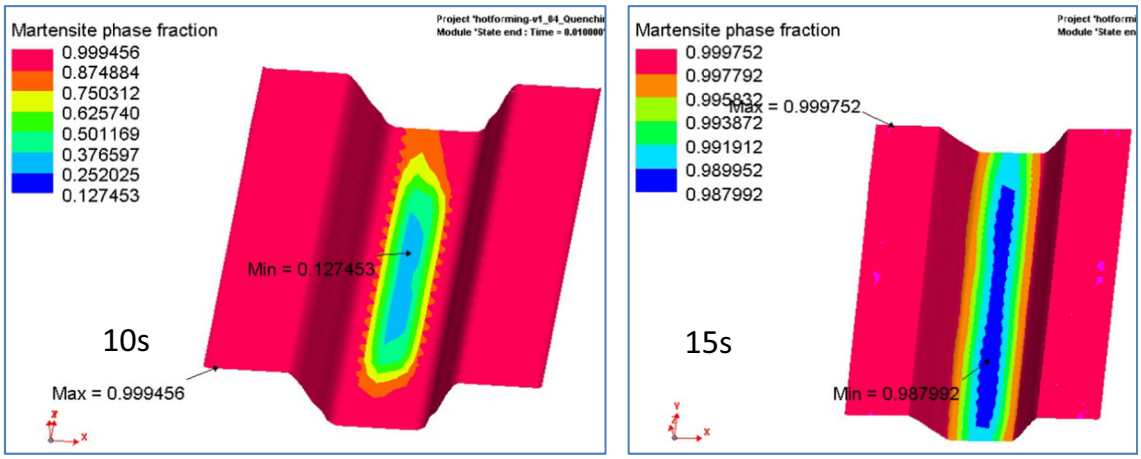

Fig. 21 Microstructure of the part at different holding and quenching time

fully in 10 s, so the initial austenitic microstructure cannot be transformed into martensite completely at the end of quenching. However, the flange of the part was almost martensite at the end of quenching with a holding time of 10 s because of the small die gap and good heat dissipation conditions. Almost full martensite was achieved with a holding time of 15 s, which indicates that the holding and quenching time should be more than 15 s in order to have a good formability and mechanical properties of the part in the V-channel hot stamping process.

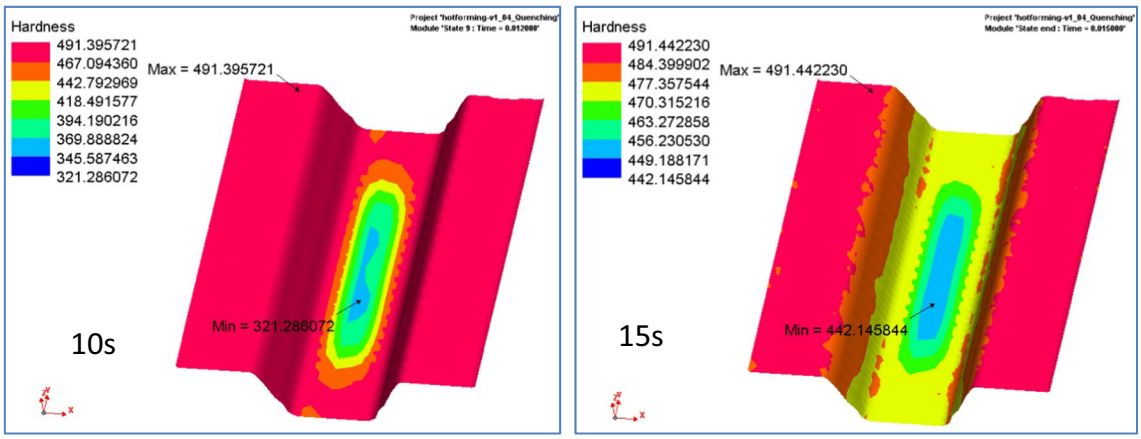

Fig. 22 Hardness of the part at different holding and quenching time

Table 3 Thinning comparison between the experiment and the simulation

Measuring positions (labeled in Fig. 8)	Thickness (mm) (measurement)	Thinning (%) (measurement)	Thinning (%) (simulation)
Bottom (1)	1.74	3.3	1.3
Bottom (2)	1.75	2.8	2.1
Sidewall (3)	1.42	21.1	25.0
Flange (4)	1.76	2.2	1.3

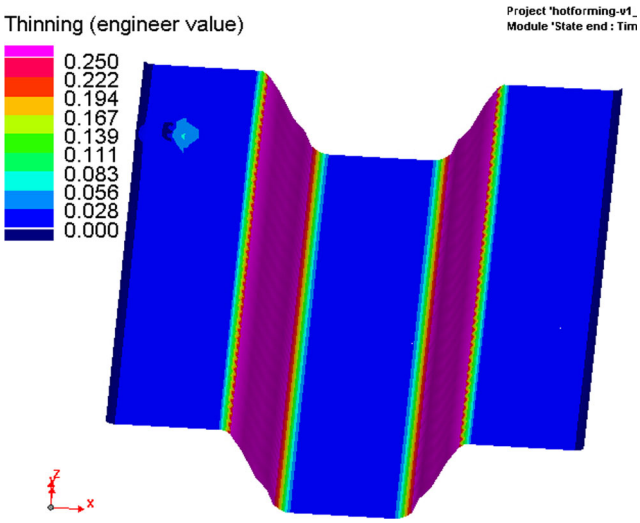

Fig. 23 Thinning of part with the initial stamping temperature of 800 °C and holding time of 15 s

4.4 Hot stamping experiment of the V-channel part

Hot stamping experiments of V-channel part were carried out with the initial stamping temperature of 800 °C and holding time of 15 s to validate the correctness of the FE modeling according to the FE simulation analysis results.

4.4.1 Tests on the thinning of the V-channel part

Tests on thinning were performed to verify the prediction results of the finite element simulation using a supersonic thickness gauge, and the testing positions are illustrated in Fig. 8. The results are listed in Table 3 and Fig. 23 shows the predictive results by FE simulation in the same conditions.

It can be seen from the test results that the sidewall of the hot-stamped part has a maximum thinning rate of 21.1 %. However, thinning rate of the bottom and flange area is only about 2 %. This is mainly related to the violently drawing deformation of the sidewall in hot stamping process, and the revealed results are corresponding to the predictive values in Fig. 23.

4.4.2 Tests on the mechanical properties and microstructure of V-channel part

In order to investigate the microstructure and mechanical properties of the hot-stamped parts, the tests on tensile strength, elongation, and hardness were carried out. Specimens for tensile tests were selected from measuring positions illustrated in Fig. 8 according to the standard GB/T 4338-2008, and the results were tabulated in Table 4.

It can be seen that the tensile strength of all testing positions is higher than 1500 MPa, which meets the using requirements of ultrahigh strength boron manganese steels, and the flange area has the highest tensile strength of 1592 MPa. Furthermore, the distribution of hardness obtained by numerical simulation shown in Fig. 24 is consistent with that obtained by the experiments. However, the values of the prediction were higher than that of measured values. It may be due to the oxide layer generated on the uncoated steel of BR1500HS during the hot stamping experiments, which results in smaller heat transfer coefficients. In addition, owing to better heat dissipation condition on flange, the hardness is bigger than that of the sidewall and bottom of the part.

When the BR1500HS steel was stamped at 800 °C, almost full martensite is transformed according to the FE simulation (Fig. 18). It can be seen from Fig. 25 that the microstructure of the testing specimens selected from bottom, sidewall, and flange area of the actual V-channel part mainly consists of full martensite with different directions. However, the relative homogeneity of the martensite was slightly different in the selected areas. The sidewall of the part cannot be fully quenched due to the die gap and poor heat dissipation condition, so the austenite cannot be transformed into martensite completely

Table 4 The comparison of mechanical properties between the experiment and the simulation

Measuring positions (labeled in Fig. 8)	Tensile strength(MPa) (measurement)	Elongation (%) (measurement)	Hardness (HV) (measurement)	Hardness (HV) (simulation)
Bottom (1)	1536	6.36	445	458
Bottom (2)	1548	6.20	440	466
Sidewall (3)	1562	7.27	476	484
Flange (4)	1592	6.30	485	491

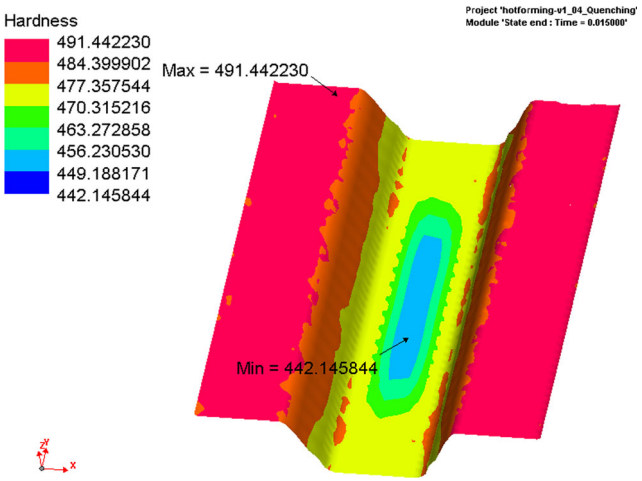

Fig. 24 Hardness of the part with the initial stamping temperature of 800 °C and holding time of 15 s

after quenching. Thus, the microstructure of the sidewall was heterogeneous distributed martensite and some bainite. Due to a good cooling condition, almost full martensite was transformed and distributed evenly in the flange of the part, which is in good agreement with the simulated results.

5 Conclusions

In the current work, the effects of strain rate and initial deformation temperature on the non-isothermal deformation behavior of BR1500HS steel were studied with a Gleeble 3500 system. Additionally, based on the stress-stain curves obtained in the non-isothermal tensile experiment and thermal-mechanical-metallurgical coupled modeling of BR1500HS steel, the FE simulation was performed to simulate the hot stamping process of a V-channel part. Finally, hot stamping experiments were carried out to validate the correctness of the FE modeling. The following major conclusions are yielded.

1. As initial deformation temperatures during non-isothermal deformation process increases, the flow stress and working hardening decrease. Compared with isothermal deformation, the forming force in non-isothermal deformation process was higher, due to more dislocations produced during non-isothermal deformation process.
2. When deformed at 750 °C, the strain rate has a more significant impact on the formability of BR1500HS steels and the test specimens were cracked even under a small amount of strain in low strain rate (0.15 s^{-1}).
3. According to the results obtained by the FE simulation, the initial stamping temperature should be above 750 °C and the holding and quenching time should be up to 15 s in hot stamping process.
4. Tests on thinning, mechanical properties, and microstructure of hot-stamped parts with initial stamping temperature of 800 °C and holding time of 15 s were carried out, and the results are in good consistency with the simulated

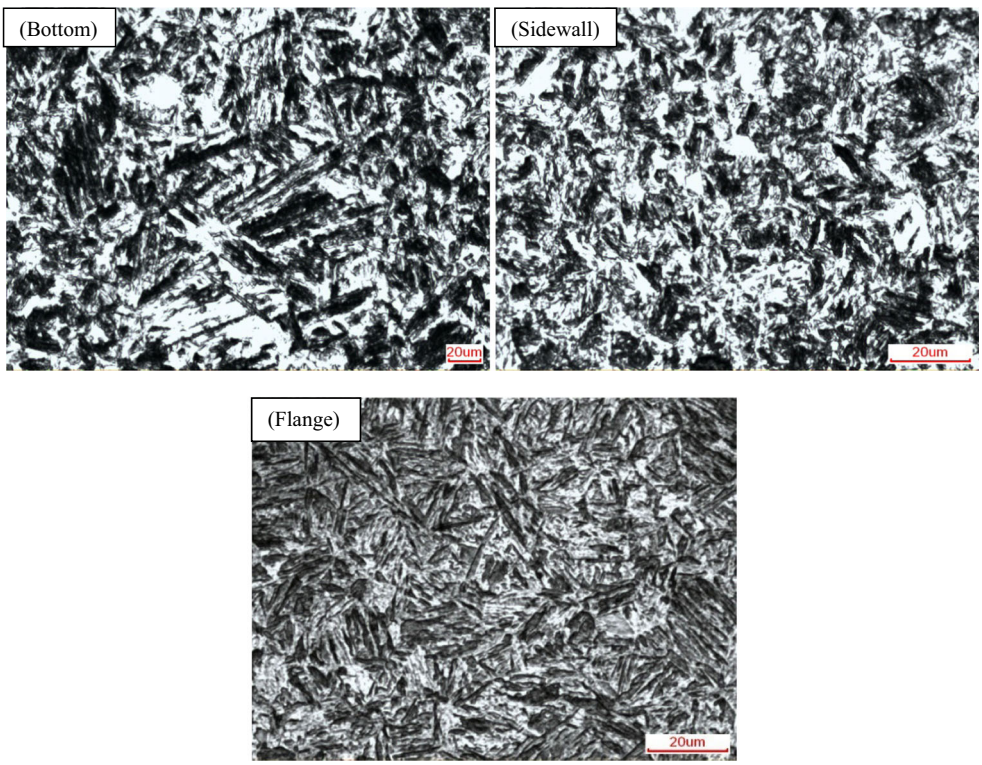

Fig. 25 Microstructure morphology of the V-channel part at selected locations labeled in Fig. 8

results. Thus, it reveals that the FE modeling of non-isothermal hot stamping process for the V-channel part built in this article is reliable.

Acknowledgments The authors would like to thank the financial support from the project of the National Natural Science Foundation of China under grant no. 51475280.

References

1. Karbasian H, Tekkaya AE (2010) A review on hot stamping. J Mater Process Technol 210:2103–2118
2. Li FF, Fu MW, Lin JP, Wang XN (2014) Experimental and theoretical study on the hot forming limit of 22MnB5 steel. Int J Adv Manuf Technol 71:297–306
3. Liu HS, Lei CX, Xing ZW (2013) Cooling system of hot stamping of quenchable steel BR1500HS: optimization and manufacturing methods. Int J Adv Manuf Technol 69:211–223
4. Naderi M, Saeed-Akbari A, Bleck W (2008) The effects of non-isothermal deformation on martensitic transformation in 22MnB5 steel. Mat Sci EnginA 487:445–455
5. Kim HY, Park JK, Lee MG (2014) Phase transformation-based finite element modeling to predict strength and deformation of press-hardened tubular automotive part. Int J Adv Manuf Technol 70:1787–1801
6. Li Y, Ying L, Hu P, Shi D, Zhao X, Dai M (2013) Coupled numerical simulation of hot stamping process and experimental verification. Aip Conf Proc 1532:471–477
7. Won CJ, Ho BH, Frédéric B, Sung SH, Jin KD, Myoung-Gyu L (2013) Experimental and numerical analyses of hot stamping parts with tailored properties. Isij Int 53:1047–1056
8. Tekkaya AE, Karbasian H, Homberg W, Kleiner M (2007) Thermo-mechanical coupled simulation of hot stamping components for process design. Prod Engin 1:85–89
9. Abbasi M, Saeed-Akbari A, Naderi M (2012) The effect of strain rate and deformation temperature on the characteristics of isothermally hot compressed boron-alloyed steel. Mat Sci Engin A 538: 356–363
10. Min J, Lin J, Min YA (2013) Effect of thermo-mechanical process on the microstructure and secondary-deformation behavior of 22MnB5 steels. J Mater Process Technol 213:818–825
11. Abbasi M, Naderi M, Saeed-Akbari A (2013) Isothermal versus non-isothermal hot compression process: a comparative study on phase transformations and structure–property relationships. Mat Des 45:1–5
12. Fan DW, Park RB, Cho YR, De Cooman BC (2010) Influence of isothermal deformation conditions on the mechanical properties Of 22Mnb5 Hpf steel. Steel Res Int 81:292–298
13. Nes E, Marthinsen K, Brechet Y (2002) On the mechanisms of dynamic recovery. Scripta Mater 47:607–611
14. Huiping L (2012) Research on the constitutive relationship of hot stamping boron steel B1500HS at high temperature. J Mech Eng 48:21–27
15. Abbasi M, Bagheri B, Ketabchi M, Haghshenas DF (2012) Application of response surface methodology to drive GTN model parameters and determine the FLD of tailor welded blank. Comput Mater Sci 53:368–376
16. Nagumo M, Matsuda H (1967) Dependence of the dislocation density on the strain rate. Jpn J Appl Phys 6:412
17. Eriksson M, Oldenburg M, Somani MC, Karjalainen LP (2002) Testing and evaluation of material data for analysis of forming and hardening of boron steel components. Model Simul Mater Sci Eng 10:277–294
18. Li HP, Gai K, He LF, Zhang CZ, Cui HZ, Li MS (2016) Non-isothermal phase-transformation kinetics model for evaluating the austenization of 55CrMo steel based on Johnson–Mehl–Avrami equation. Mater Des 92:731–741
19. Lidam RN, Manurung YHP, Haruman E, Redza MR, Rahim MR, Sulaiman MS, Zakaria MY, Tham G, Abas SK, Chau CY (2013) Angular distortion analysis of the multipass welding process on combined joint types using thermo-elastic–plastic FEM with experimental validation. Int J Adv Manuf Technol 69:2373–2386